

CrystEngComm

Accepted Manuscript



This is an *Accepted Manuscript*, which has been through the Royal Society of Chemistry peer review process and has been accepted for publication.

Accepted Manuscripts are published online shortly after acceptance, before technical editing, formatting and proof reading. Using this free service, authors can make their results available to the community, in citable form, before we publish the edited article. We will replace this *Accepted Manuscript* with the edited and formatted *Advance Article* as soon as it is available.

You can find more information about *Accepted Manuscripts* in the [Information for Authors](#).

Please note that technical editing may introduce minor changes to the text and/or graphics, which may alter content. The journal's standard [Terms & Conditions](#) and the [Ethical guidelines](#) still apply. In no event shall the Royal Society of Chemistry be held responsible for any errors or omissions in this *Accepted Manuscript* or any consequences arising from the use of any information it contains.

Combustion Synthesis and Excellent Photocatalytic Degradation Properties of $W_{18}O_{49}$

Pengqi Chen,^{a,*} Mingli Qin,^a Dezhi Zhang,^b Zheng Chen,^a Baorui Jia,^a Qi Wan,^c Haoyang

Wu,^a Xuanhui Qu,^a

^a School of Materials Science and Engineering, University of Science and Technology

Beijing, Beijing 100083, China

^b Aerospace Research Institute of Materials & Processing Technology, Beijing

100076, China

^c Energy Material & Technology Research Institute, General Research Institute for

Nonferrous Metal, Beijing 100088, China

Corresponding author: pengqichen@163.com (Pengqi Chen); Tel: +86-10-82375859; Fax:

+86-10-62334311.

In this paper, one-dimensional $W_{18}O_{49}$ nanopowders were fabricated by a one-step solution combustion method using glycine as the fuel and metal acid radical ion as the metal source. The morphologies and non-stoichiometric single-crystal phase of $W_{18}O_{49}$ can be controlled by changing the amount of the fuel. The nanoneedles had large amount of defects such as oxygen vacancies. This characteristic resulted in an excellent visible driven photocatalytic performance that it took about 50 min to degrade the methylene blue (100 mL; 40 mg•L⁻¹) under visible light. The interesting reaction mechanism of such needle-like $W_{18}O_{49}$ and photocatalytic mechanism are studied in this paper.

As energy shortages and environmental pollution raise awareness of a potential

global crisis, researchers have done many works and find photocatalysis with oxide semiconductor (TiO_2 ¹, ZnO ², Fe_2O_3 ³, and WO_{3-x} ⁴, etc.) is one of the most promising technologies. Among tungsten oxide (WO_{3-x}), $\text{W}_{18}\text{O}_{49}$ has been extensively studied due to its unusual defect structures and novel properties in the nanometer regime, which allow it to be an effective candidate in various applications. Monoclinic $\text{W}_{18}\text{O}_{49}$ with the largest oxygen deficiency in $\text{WO}_{2.7}\text{--}\text{WO}_3$ is reported as the only oxide isolated in a single phase, different from other tungsten sub-oxides.⁵ This characteristic endows $\text{W}_{18}\text{O}_{49}$ with better conductivity, which can be assembled for electrochromic devices and smart supercapacitor.⁶⁻⁸ Since $\text{W}_{18}\text{O}_{49}$ consists of mixed valence tungsten ions and can absorb the near infrared ray, it has been used as superior heat-insulating film to save energy.⁹ Furthermore, with a wide absorption tail in visible region, $\text{W}_{18}\text{O}_{49}$ has been viewed as a promising visible photocatalyst for many organic pollutants. For example, it shows unexpected capability in photocatalytic dehydration of IPA to propylene under visible light irradiation.¹⁰⁻¹²

Previously, several methods have been used to synthesize nanoscale $\text{W}_{18}\text{O}_{49}$ powder such as thermal decomposition, hydrothermal method, thermal oxidation of tungsten and bioligand-assisted method.¹¹⁻¹⁴ Bai and co-workers¹⁰ used a surfactant-free alcoholthermal method for the synthesis of a self-assembled $\text{W}_{18}\text{O}_{49}$ network possessing high oxygen vacancy concentration. Huang et al¹⁵ used solvothermal treatment to synthesize urchin- and nanowire-like $\text{W}_{18}\text{O}_{49}$ with high photocatalytic activity. But these methods took a long time and the resultant powders had to be centrifuged for the selection, which was complicated. Hence, it is important

to develop a novel energy-efficient synthesis route for $W_{18}O_{49}$.

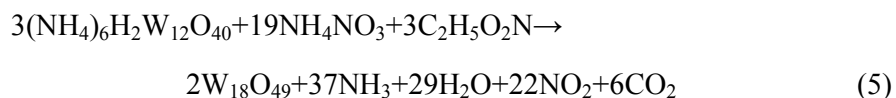
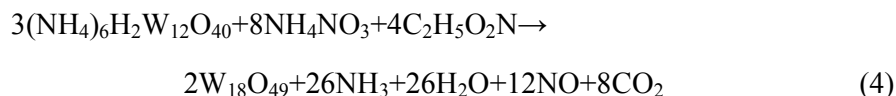
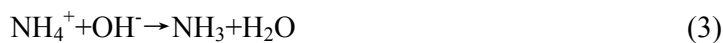
Solution combustion synthesis (SCS) is demonstrated to be a versatile and energy-efficient method for preparing inorganic oxide semiconductors. This low-temperature combustion synthesis can obviously shrink the energy payback time, which is a key parameter in life cycle analyses of solar energy materials and devices.⁴ What is more, this method is time and cost efficient, and can achieve the products with different morphologies and composition in one step.¹⁶⁻¹⁸ Morales et al⁴ prepared WO_3 powders by combustion synthesis, but using this method to synthesize $W_{18}O_{49}$ has never been reported. This is because $W_{18}O_{49}$ has a very narrow stoichiometric range in the binary phase diagram of tungsten and oxygen and the combustion synthesis of tungsten oxides with lower oxidation states is not easy to be realized. Hence, in this communication, we proposed the combustion synthesis of $W_{18}O_{49}$ nanoneedles by using glycine for the first time.

In the combustion reaction, we used metal acid radical ion ($[H_2W_{12}O_{40}]^{6-}$) as the metal source which was different from the traditional solution combustion synthesis, where metal cation salt was often used. And glycine and ammonium nitrate were selected as the fuel and oxidizer, respectively. In a typical experiment, 0.01 mol ammonium paratungstate, 0.24 mol ammonium nitrate and 0.1 mol glycine were dissolved in 150 ml deionized water. With heating the solution evaporated to paste and later on this mixture foamed due to the generation of gaseous decomposition products and led to enormous swelling. These gases were known to be hypergolic in contact with each other. At last the foam burned with a flame when the gases and

energy were sufficient. The combustion products we got were violet powders. Because the reaction was conducted in a fuel-rich condition, we did not need extra atmospheric oxygen to promote the reaction. Simultaneously, a large amount of gases (NH₃, H₂O, NO, etc.) generated by heating created an oxygen-deficient environment, in which [H₂W₁₂O₄₀]⁶⁻ was reduced into W₁₈O₄₉ nucleus by the excessive amounts of NH₃.²¹ That is a great advantage of our synthesis method.

To obtain a good understanding of the solution combustion synthesis process, we characterized this reaction by using thermogravimetry (TG)-differential scanning calorimetry (DSC) coupled with a mass spectrometer. These experiments were carried out from room temperature to 400 °C at a heating rate of 10 °C·min⁻¹ in air. Figure 1(a) shows that there is presence of small endothermic peak at 134 °C accompanied with ~4% weight loss which is attributed to vaporization of chemical absorbed water. Another endothermic peak at 170 °C may come from the decomposition of NH₄NO₃. And the abrupt weight loss with a huge exothermic peak occurring around 230 °C is caused by the combustion of the reactive gel. No more weight loss is seen after combustion. The mass spectroscopy (MS) analysis (Figure 1(b)) also shows similar results with the two stages. In the first stage, the formed gases are NH₃, and H₂O, and then in the second stage the gases released during the fast process contained NH₃, H₂O, NO, CO₂, and NO₂, which mainly originated from the intermolecular complex reactions concluding decomposition and redox.^{19, 20} The total sequence of reactions are presented as follows:





The X-ray diffraction pattern (XRD) enables us to investigate the structure and phase of the product. In figure 2(a) the pattern could be indexed to the well-crystalline, monoclinic $\text{W}_{18}\text{O}_{49}$ (JCPDS No. 84-1516) with the lattice parameters of $a=18.318$, $b=3.783$, $c=14.028$ Å. The close-packed diffraction peaks (010) and (020) are in agreement with the XRD pattern of $\text{W}_{18}\text{O}_{49}$ reported in the paper,²² which suggests that the possible crystal growth direction of the sample is (010). The pure monoclinic $\text{W}_{18}\text{O}_{49}$ has a distorted ReO_3 structure that consists of a highly anisotropic lattice of edge-sharing WO_6 octahedra.^{10, 12} The field emission scanning electron microscopy (FESEM) image (figure 2(b)) shows the morphology of nanoneedle $\text{W}_{18}\text{O}_{49}$, and the nanoneedles are ~ 80 nm in diameter and ~ 5 μm in length. The energy-dispersive X-ray (EDS) analysis also confirms the presence of $\text{W}_{18}\text{O}_{49}$ (see in figure S1).

The detail information of the $\text{W}_{18}\text{O}_{49}$ nanoneedles (figure.3(a)) is intensively studied by transmission electron microscope (TEM). TEM image (figure.3(b)) shows that the diameter of a single $\text{W}_{18}\text{O}_{49}$ nanoneedle is approximately 40 nm. The single-crystalline nature of the $\text{W}_{18}\text{O}_{49}$ nanoneedle is evidenced by the same high resolution transmission electron microscopy (HRTEM) image and selected-area electron diffraction (SAED) pattern shown in figure.3(c) and (d), respectively. The

spacing of lattice planes is measured to be 0.38 nm, which could be indexed as (010) of the monoclinic $W_{18}O_{49}$. Because the $W_{18}O_{49}$ lattice is built up of WO_6 octahedra coupled with each other in an intricate way by sharing corners and edges,²³ the fastest growth rate is probably achieved by linking these octahedra to form linear rows. Then the growth is preferentially along the nanowire axis with defects propagating along the nanowire length. Therefore, it can be concluded that the crystal grew along the (010) direction.^{24, 25} What is more, transverse displacements of the atomic columns across the defect plane are evident along the growth direction (red box in figure. 3(c)). This kind of stacking faults exists in the entire length of the needle, due to the O substoichiometry.^{21, 23} And in SAED patterns, the extension streaking of the diffraction spots perpendicular to the nanoneedle axis also indicates the presence of unequally spaced planar defects, which is similar to other works^{21, 23}.

The surface electronic structure and elemental valence of $W_{18}O_{49}$ are assessed by X-ray photoelectron spectroscopy (XPS). The figure 4(a) shows the full range of XPS spectra of the powder, and figure 4(b) shows the narrow scan XPS spectra of W element. For the tungsten, the W 4f spectrum could be deconvoluted into three doublets as shown. The two peaks at 37.8 and 35.7 eV are assigned to the binding energies of W^{6+} , and other two peaks observed at 36.9 and 34.7 eV correspond to W^{5+} . According to the literature²⁶, the structure of the $W_{18}O_{49}$ has some rather short W-W distances of 0.26 nm and the removal of oxygen occurs at the shear planes. So there are the places where W^{5+} is likely to be formed. The third doublet, with a lowest binding energy at 33.7 and 35.8 eV, results from emission of W $4f_{5/2}$ and W $4f_{7/2}$ core

levels from the atoms in an oxidation state of 4+. And the presence of W^{4+} can be explained by assuming a dismutation of a part of W^{5+} . The W^{4+} ions are linked with the W-W distances. These three oxidation states are the typical non-stoichiometric characteristics of $W_{18}O_{49}$ nanomaterials.^{27,28}

In order to give a more clear understanding of this synthesis, we have also conducted a series of experiments. We added different amounts of glycine (0 mol, without fuel condition, 0.05mol, stoichiometric equilibrium condition, 0.2 mol, fuel-rich condition, details in supporting information) in the reaction system and found that the reaction was changed. The figure 5(d) shows the XRD analysis of the products. It is observed that the synthesized sample without glycine (line 1) is composed of tungsten oxide hydrate ($WO_3 \cdot 0.33H_2O$, orthorhombic, JCPDS No. 54-1012) and hydrotungstite ($H_2WO_4 \cdot H_2O$, monoclinic, JCPDS No. 18-1420). When the glycine increased to 0.05 mol, the line (2) shows the phase change into pure orthorhombic WO_3 . For line (3), with 0.2 mol glycine, the diffraction peaks of the powder are indexed to monoclinic $W_{18}O_{49}$ and monoclinic WO_3 . Therefore, an appropriate amount of glycine is necessary for the synthesis of pure $W_{18}O_{49}$.

As the change of phase composition showed in XRD analysis, the morphology and structure of the products also have significant difference with the change of the glycine amount. In figure 5(a), the sample synthesized without glycine is an urchin-like structure assembled by nanorods and nanoparticles, which comes from the exothermic decomposition of the mixed mass as indicated in TG–DSC analysis (figure S2). Figure 5(b) gives the characterization of the sample synthesized with

0.05 mol glycine. In the reaction the precursor won't swell to the foam and the gases produced by the redox reaction are a little, the powders generate in the system with sufficient oxidizing agent. So it is found that the particles have the diameter of 100~200nm and the agglomeration exists obviously. As shown in figure 5(c), the sample synthesized with 0.2 mol glycine is composed nanoparticles and nanorods. The diameter of the nanorods is about 250 nm, much larger than that of the nanoneedles synthesized with 0.1 mol glycine. Obviously, adding more glycine makes the combustion reaction more vigorous, even leading to eruption combustion synthesis. It will generate an environment which has higher combustion temperature.¹⁶ In this case, the product will be shorter and thicker. And the $W_{18}O_{49}$ powders are partly oxidized into WO_3 when exposed in air at high temperature after the gases releasing over. So the powder we get finally is the mixture of WO_3 and $W_{18}O_{49}$.

Our final evaluation of the $W_{18}O_{49}$ powder synthesized by SCS is to measure the photocatalytic ability. The $W_{18}O_{49}$ nanoneedles show high photocatalytic activity, as indicated in the visible and near infrared absorption spectroscopy (figure 6(a)). Obviously, a very large absorption tail in the visible and near infrared (NIR) regions gives evidence that the $W_{18}O_{49}$ nanoneedles consist of a large number of oxygen vacancies,^{20, 29} corresponding to the results of TEM analysis. And then we used methylene blue (MB) as a model contaminant for photocatalytic decolorization. This dye is a popular probe and its "dark" adsorption and subsequent decomposition can be monitored via its visible-light absorption signature. What is more, we added hydrogen

peroxide (H_2O_2) as electron acceptor. The insert data in figure 6(b) shows that the as-synthesized $\text{W}_{18}\text{O}_{49}$ reaches the adsorption equilibrium in dark after 30 min and that 96% of the initial concentration still remained in the solution. When the light was turned on, the characteristic peak diminished sharply with the increasing irradiation time, and the color of dye solution changed from blue to colorless after about 50 min. In recent researches, S. Bai et al³⁰ showed that it took 75 min to degrade the 100% of Rhodamine B., Fumi and co-workers¹¹ used the carbon-coated $\text{W}_{18}\text{O}_{49}$ prepared by the heat treatment of the powder mixtures to degrade the MB. Although it would accelerate photocatalysis process, it still need several hours to complete it. Compared with their works, we can prepared the material by an effective method with simple experimental setup and significant time saving. What is more, to eliminate the self-degradation of MB under interior irradiation, we performed an experiment without $\text{W}_{18}\text{O}_{49}$ under the same conditions for comparison. The concentration of MB was changed weekly. (details in S2)

The figure 6(b) presents the ratio of degradation versus irradiation time. The results reveal that the presence of the $\text{W}_{18}\text{O}_{49}$ nanostructures catalyst increases the degradation process significantly. This enhancement may be attributed to the suitable band gap and large quantities of defects. In our case, the electron-hole pairs are generated in the conduction band (CB) and valance band (VB) of $\text{W}_{18}\text{O}_{49}$ upon UV-Visible light illumination, respectively. And then the photogenerated electrons are trapped by H_2O_2 that formed active hydroxy radicals ($\cdot\text{OH}$), which subsequently degrades the organic dye.³¹⁻³³

Conclusions

In summary, monoclinic $W_{18}O_{49}$ nanoneedles were synthesized via ultra-rapidly solution combustion synthesis method with low-cost, non-toxic starting materials. And the TEM, XPS and TG-MS measurements revealed the interesting reaction mechanism of $W_{18}O_{49}$ nanoneedles. As was evidenced, the amount of glycine played a vital role in synthesis of $W_{18}O_{49}$, and the high-pure powder could be prepared under the condition of 0.1 mol glycine adding. The synthesized $W_{18}O_{49}$ showed a considerable rate for organic degradation under UV-visible light. This work presents a possibility for the use of $W_{18}O_{49}$ nanoneedles as a functional material in the degradation of organic pollutants. And the results suggest that it may be possible that solution combustion synthesis can be used as a new strategy to design materials with oxygen-vacancy-rich nonstoichiometric simple oxides.

Acknowledgments

This work is financially supported by the National Natural Science Foundation Program of China (50802006) and (51172017), Natural Science Foundation Program of Beijing (2102028).

References:

- [1] J. Schneider, M. Matsuoka, M. Takeuchi, J. Zhang, Y. Horiuchi, M. Anpo and D. W. Bahnemann, *Chem. Rev.*, 2014, **114**, 9919-9986.
- [2] N. Gogurla, A. K. Sinha, S. Santra, S. Manna and S. K. Ray, *Scientific Reports*.

2014, 4.

[3] H. Sun, L. Cao and L. Lu, *Nano Res.*, **2011**, 4, 550.

[4] W. Morales, M. Cason, O. Aina, N. R. de Tacconi, and K. Rajeshwar, *J. Am. Chem. Soc.*, **2008**, 130(20): 6318-6319.

[5] M. Remškar, J. Kovac, M. Viršek, M. Mrak, A. Jesih and A. Seabaugh, *Adv. Func. Mater.*, **2007**, 17(12), 1974-1978.

[6] S. Yoon, E. Kang, J. K. Kim, C. W. Lee and J. Lee, *Chem. Commun.*, **2011**, 47, 1021–1023.

[7] Y. Tian, S. Cong, W. Su, H. Chen, Q. Li, F. Geng and Z. Zhao, *Nano letters*, **2014**, 14(4): 2150-2156.

[8] J. W. Liu, J. Zheng, J. L. Wang, J. Xu, H. H. Li and S. H. Yu, *Nano Lett.*, **2013**, 13(8), 3589-3593.

[9] C. Guo, S. Yin, Y. Huang, Q. Dong and T. Sato, *Langmuir*, **2013**, 27(19), 12172-12178.

[10] H. Bai, N. Su, W. Li, X. Zhang, Y. Yan, P. Li, S. Ouyang, J. Ye and G. Xi, *J. Mater. Chem. A*, **2013**, 1(20), 6125-6129.

[11] F. Kojin, M. Mori, T. Morishita and M. Inagaki, *Chem. Lett.*, **2006**, 35(4), 388-389.

[12] G. Xi, S. Ouyang, P. Li, J. Ye, Q. Ma, N. Su, H. Bai and C. Wang, *Angew. Chem. Int. Ed.*, **2012**, 51(10), 2395-2399.

[13] A. Watchenrenwong, W. Chanmanee, N. R. de Tacconi, C. R. Chenthamarakshan, P. Kajitvichyanukul and K. Rajeshwar, *J. Electroanal. Chem.* **2008**, 612, 112.

- [14] J. Polleux, N. Pinna, M. Antonietti, M. Niederberger, *J. Am. Chem. Soc.* **2005**, 127, 15595-15601.
- [15] Z. F. Huang, J. Song, L. Pan, F. Lv, Q. Wang, J. J. Zou, X. Zhang and L. Wang, *Chem. Commun.*, **2014**, 50(75), 10959-10962.
- [16] W. Wen and J. M. Wu. *ACS Appl. Mater. Interfaces*, **2011**, 3(10): 4112-4119.
- [17] K. Rajeshwar and N. R. de Tacconi. *Chem. Soc. Rev.*, **2009**, 38(7): 1984-1998.
- [18] K. V. Manukyan, A. Cross, S. Roslyakov, S. Rouvimov, A. S. Rogachev, E. E. Wolf and A. S. Mukasyan, *J. Phys. Chem. C*, **2013**, 117(46): 24417-24427.
- [19] J. Li, Z. Wang, X. Yang, L. Hu, Y. Liu and C Wang, *J. Anal. Appl. Pyrolysis*, **2007**, 80(1): 247-253.
- [20] K. V. Manukyan, A. Cross, S. Roslyakov, S. Rouvimov, A. S. Rogachev, E. E. Wolf and A. S. Mukasyan, *J. Phys. Chem. C*, **2013**, 117(46), 24417-24427.
- [21] A. M. Smith, M. G. Kast, B. A. Nail, S. Aloni and S. W. Boettcher, *J. Mater. Chem. A*, **2014**, 2(17), 6121-6129.
- [22] K. Lee, W. S. Seo and J. T. Park, *J. Am. Chem. Soc.*, **2003**, 125(12), 3408-3409.
- [23] J. Zhou, Y. Ding, S. Z. Deng, L. Gong, N. S. Xu and Z. L. Wang, *Adv. Mater.*, **2005**, 17, 2107-2110.
- [24] X. Yan, D. Xu and D. Xue, *Acta Mater.*, **2007**, 55(17), 5747-5757.
- [25] X. Zhao, Z. Bao, C. Sun and D. Xue, *J. Cryst. Growth*, **2009**, 311(3), 711-715.
- [26] B. A. De Angelis and M. Schiavello, *J Solid State Chem*, 1977, **21**, 67-72.
- [27] S. Jeon and K. Yong, *Nanotechnol.*, **2007**, 18(24), 245602.
- [28] G. Leftheriotis, S. Passacantando, P. Yianoulis and A. Siokou, *Thin Solid Film*,

2001, 384, 298.

[29] T. Nütz and M. Haase, *J. Phys. Chem. B*, **2000**, 104(35), 8430-8437.

[30] S. Bai, Kewei Zhang, J. Sun, R. Luo, D. Li and A. Chen, *Crystengcomm*, 2014, **16**, 3289-3295.

[31] R. Abe, H. Takami, N. Murakami and B. Ohtani, *J. Am. Chem. Soc.*, **2008**, 130, 7780.

[32] X. Chang, L. Dong, Y. Yin and S. Sun, *RSC Advances*, **2013**, 3(35), 15005-15013.

[33] X. Zhang, X. Lu, Y. Shen, J. Han, L. Yuan, L. Gong, Z. Xu, X. Bai, M. Wei, Y. Tong, Y. Gao, J. Chen, J. Zhou and Z. L. Wang, *Chem. Commun.*, **2011**, 47(20), 5804-5806.

Figure captions

Fig. 1 Results of (a) TG–DSC and (b) MS analysis for the reaction with 0.1 mol glycine.

Fig. 2 (a) XRD patterns and (b) FESEM image of the powder synthesized with 0.1 mol glycine, respectively.

Fig. 3 TEM images of $W_{18}O_{49}$. (a) low magnification, (b) a single nanoneedle, (c) HRTEM image and (d) SAED pattern, respectively.

Fig. 4 XPS spectra of $W_{18}O_{49}$ nanoneedles (a) full range XPS spectra (b) W4f core-level spectrum with peaks corresponding to W^{6+} , W^{5+} , W^{4+} .

Fig. 5 FESEM images of the products synthesized with (a) 0 mol, (b) 0.05 mol, (c) 0.2 mol glycine, and (d) XRD patterns of the products synthesized with (1) 0 mol, (2) 0.05 mol, (3) 0.2 mol glycine respectively.

Fig. 6 (a) Optical absorption spectrum of the $W_{18}O_{49}$ powder. (b) Plot of degradation C_t/C_0 as a function of irradiation time. Inset shows the changes of time-dependent UV-Vis absorbance spectra in the presence of $W_{18}O_{49}$ under visible-light irradiation for different times.

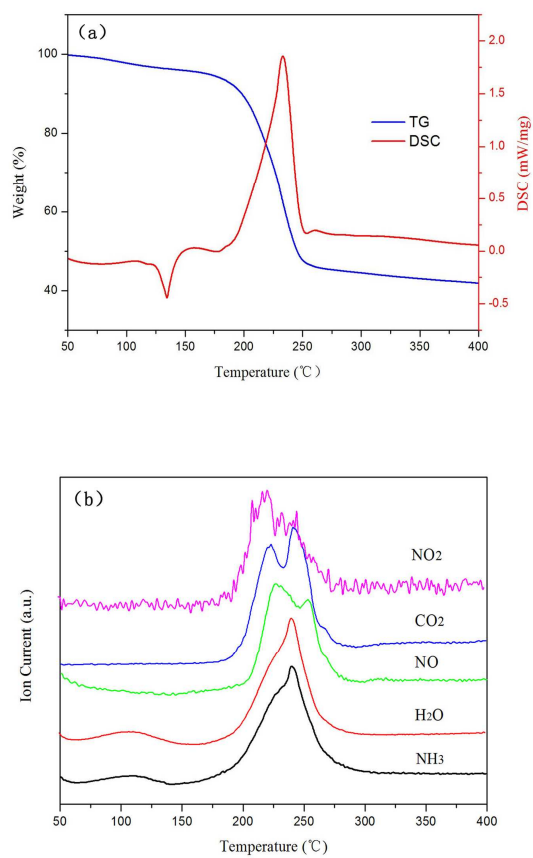
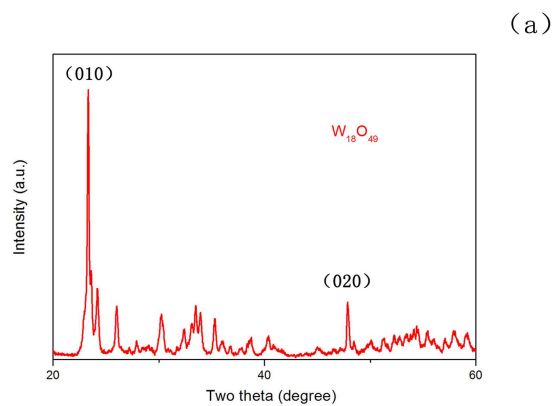


Fig.1



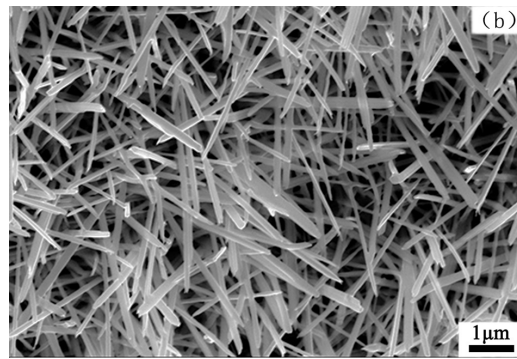


Fig.2

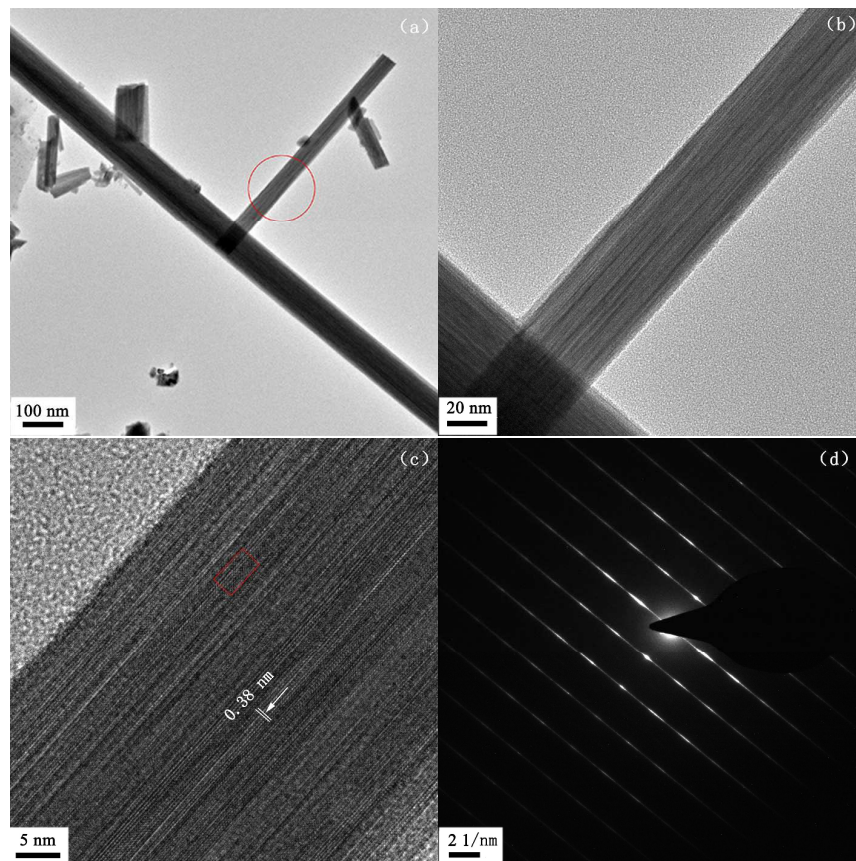


Fig.3

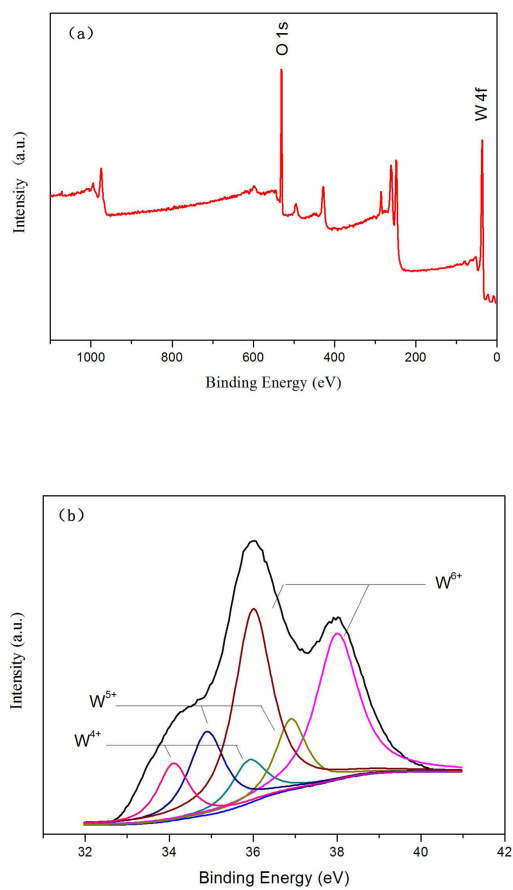


Fig. 4

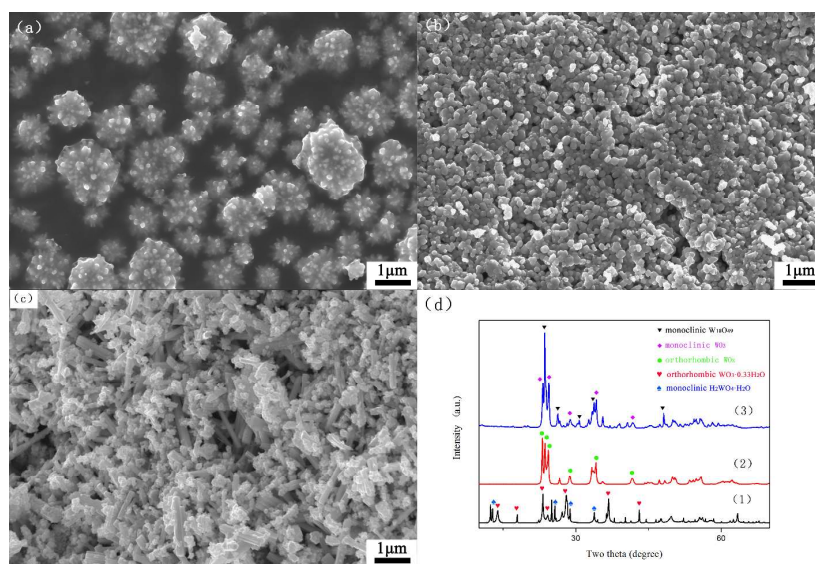


Fig.5

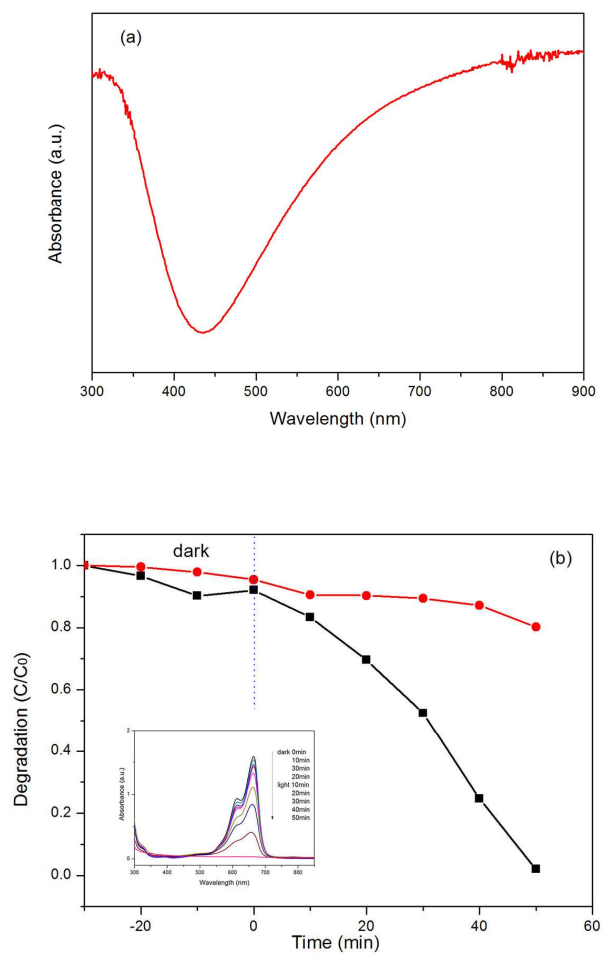
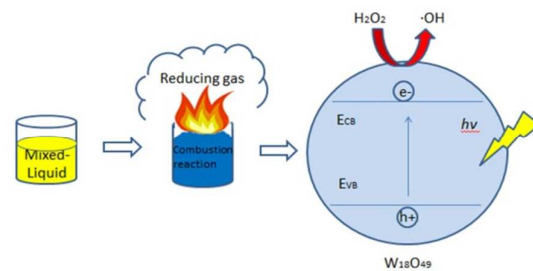


Fig.6



One-dimensional $W_{18}O_{49}$ nanoneedles were fabricated by solution combustion synthesis and exhibited an excellent visible driven photocatalytic performance.